© 2016. Published by The Company of Biologists Ltd | Journal of Cell Science (2016) 129, 804-816 doi:10.1242/jcs.176750

RESEARCH ARTICLE

SMN affects membrane remodelling and anchoring of the protein synthesis machinery

Francesca Gabanella[1,2], Cinzia Pisani[3], Antonella Borreca[1,2], Stefano Farioli-Vecchioli[1,2], Maria Teresa Ciotti[1,4], Tiziano Ingegnere[5,*], Annalisa Onori[3], Martine Ammassari-Teule[1,2], Nicoletta Corbi[3], Nadia Canu[1,6], Lucia Monaco[7], Claudio Passananti[3] and Maria Grazia Di Certo[1,2,‡]

ABSTRACT

Disconnection between membrane signalling and actin networks can have catastrophic effects depending on cell size and polarity. The survival motor neuron (SMN) protein is ubiquitously involved in assembly of spliceosomal small nuclear ribonucleoprotein particles. Other SMN functions could, however, affect cellular activities driving asymmetrical cell surface expansions. Genes able to mitigate SMN deficiency operate within pathways in which SMN can act, such as mRNA translation, actin network and endocytosis. Here, we found that SMN accumulates at membrane protrusions during the dynamic rearrangement of the actin filaments. In addition to localization data, we show that SMN interacts with caveolin-1, which mediates anchoring of translation machinery components. Importantly, SMN deficiency depletes the plasma membrane of ribosomes, and this correlates with the failure of fibroblasts to extend membrane protrusions. These findings strongly support a relationship between SMN and membrane dynamics. We propose that SMN could assembly translational platforms associated with and governed by the plasma membrane. This activity could be crucial in cells that have an exacerbated interdependence of membrane remodelling and local protein synthesis.

KEY WORDS: SMN, Local translation, Membrane remodelling, Actin filament

INTRODUCTION

The establishment of cell polarity depends on the ability to dissect functional subcellular domains in response to intrinsic developmental programmes or external stimuli (Wodarz, 2002; Bryant and Mostov, 2008). An advantageous mechanism to select the protein profile both in space and in time is the asymmetrical distribution or translation of mRNAs (Besse and Ephrussi, 2008; Medioni et al., 2012; Xing and Bassell, 2013; Jung et al., 2014). At least two factors contribute to restricting protein synthesis to discrete compartments: the highly oriented cytoskeletal network, and the packaging of mRNAs into dedicated ribonucleoprotein particles (mRNPs) (Holt and Bullock, 2009; Xing and Bassell, 2013). Furthermore, membrane receptor signalling provides essential inputs to ensure a fine-tuning of the cytoplasmic control of gene expression (Latham et al., 1994; Willis et al., 2007; Ridley, 2011). Signal transduction pathways, such as the mammalian target of rapamycin (mTOR) signalling cascade, switch receptor activity into localized translational outputs by activating components of translation machinery (Berven et al., 2004; Hoeffer and Klann, 2010). Notably, an elegant work has highlighted the ability of the plasma membrane to govern local protein synthesis not only as mediator of extracellular cues (Tcherkezian et al., 2010). The authors showed that the plasma membrane of neural cells sequesters inactive components of translation machinery, including the 40S and 60S ribosomal subunits. In an activity-dependent manner, ribosomes are released from the plasma membrane and are recruited into translating polyribosomes, to promote spatially restricted protein production. Furthermore, a great deal of progress has been made in identifying mechanisms that regulate the local translation, revealing RNA-binding proteins involved in the sorting or translation of mRNAs (Xing and Bassell, 2013). Some of these, such as the zipcode-binding protein 1 (ZBP1) and the KH domain-containing splicing regulatory protein (KSRP, also known as KHSRP), contact the mRNA upon transcription or splicing (Pan et al., 2007; Holt and Bullock, 2009). Other RNA-binding proteins, such as the fragile X mental retardation protein (FMRP, also known as FMR1) and the fused in sarcoma protein (FUS), affect their target transcripts preferentially at the translational level (Napoli et al., 2008; Darnell et al., 2011; Yasuda et al., 2013). Consistent with the crucial role of the local protein synthesis in the generation of cell polarity, the genetic alterations of RNA-related proteins have been linked to severe neurological disorders (Bassell and Warren, 2008; Kwiatkowski et al., 2009).

The survival motor neuron (SMN) protein is known to be involved in important tasks of RNA metabolism (Li et al., 2014). In humans, two almost identical genes, *SMN1* and *SMN2*, encode SMN protein. Although *SMN1* produces full-length transcripts, *SMN2* mainly produces an alternatively spliced mRNA, whose product is rapidly degraded. As a consequence, *SMN2* can not compensate for *SMN1* defects, unless *SMN2* is present in multiple copies. Mutations of *SMN1* result in spinal muscular atrophy (SMA), the leading genetic cause of infant mortality (Hamilton and Gillingwater, 2013). The complete loss of SMN is not compatible with the cell viability in all tissue types, whereas reduced SMN levels affect cells differentially. The large α-motoneurons in the spinal cord display the highest susceptibility to SMN deficiency, but the molecular mechanism underlying this selectivity remains obscure. To date, the best-characterized function of SMN is the cytoplasmic assembly of the small nuclear RNPs (snRNPs), the core components of the pre-mRNA splicing machinery (Pellizzoni et al., 2002). However, an emerging idea is that the loss of additional

[1]CNR-Institute of Cell Biology and Neurobiology, Rome 00143, Italy. [2]IRCCS Fondazione Santa Lucia, Rome 00143, Italy. [3]CNR-IBPM, Department of Molecular Medicine, Sapienza University of Rome, Rome 00161, Italy. [4]European Brain Research Institute (EBRI) Rita Levi-Montalcini, Rome 00143, Italy. [5]Department of Ecological and Biological Sciences, Tuscia University, Viterbo 01100, Italy. [6]Department of System Medicine, University of 'Tor Vergata', Rome 00137, Italy. [7]Department of Physiology and Pharmacology, Sapienza University of Rome, Rome 00185, Italy.
*Present address: IRCCS Regina Elena National Cancer Institute, Rome 00144, Italy.

[‡]Author for correspondence (mariagrazia.dicerto@cnr.it)

Received 30 June 2015; Accepted 29 December 2015

Journal of Cell Science

Journal of Cell Science (2016) 129, 804-816 doi:10.1242/jcs.176750

function(s) of SMN unrelated to RNA splicing could co-contribute to SMA pathogenesis. In particular, it has been strongly suggested that SMN is involved in the trafficking and/or translation of target transcripts (Rossoll et al., 2003; Tadesse et al., 2008; Glinka et al., 2010; Peter et al., 2011; Hubers et al., 2011; Fallini et al., 2011, 2014; Yamazaki et al., 2012; Rathod et al., 2012; Sanchez et al., 2013). In this context, it is noteworthy to mention cross-species conserved genes able to mitigate the SMN loss-of-function defects (Dimitriadi et al., 2010). Among others, the modifier gene plastin 3 (*PLS3*) has been shown to protect fully against deficiency in SMA (Oprea et al., 2008). PLS3 is an F-actin-bundling protein, primarily involved in the regulation of the actin cytoskeleton (Delanote et al., 2005). Interestingly, zebrafish SMN mutants display reduced PLS3 protein production, without changes at the transcriptional level (Hao et al., 2012). Importantly, proteins encoded by SMA modifier genes operate within distinct cellular networks, specifically, actin dynamics, endocytosis and mRNA translational control (Dimitriadi et al., 2010). These apparently dissimilar pathways might act in concert, and their perfect coupling might converge on the generation and maintenance of cell polarity (Gibbings et al., 2009; Lee et al., 2009; De Rubeis et al., 2013). Collectively, these findings prompted us to investigate a possible involvement of SMN at the functional interplay between actin dynamics and translational control networks.

In this study, we provide evidence for an intimate link between SMN and plasma membrane dynamics. We found that SMN interacts with caveolin-1, a key regulator of plasma membrane composition and expansion. We demonstrate that SMN coexists with translation machinery components in caveolin-rich membrane domains. Importantly, SMN deficiency depletes the plasma membrane of ribosomal proteins, and this correlates with the impairment of actin and membrane remodelling. In conclusion, our findings reveal a possible involvement of SMN in local protein production underlying plasma membrane-actin network axis.

RESULTS

Subcellular distribution of SMN during actin remodelling

All membrane protrusions known to occur at the leading edge of the cell, such as lamellipodia and filopodia, are dynamically orchestrated by changes in the polymerization and assembly of the actin cytoskeleton (Ridley, 2011). In order to explore a functional link between SMN and actin dynamics, we subjected fibroblasts to an ATP depletion and recovery assay. This approach stimulates the extension of actin-based membrane protrusions, and provides a useful tool to address key determinants of the actin network in living cells (Svitkina et al., 1986; Bear et al., 2002). In our system, after 30 min of ATP recovery, ∼70% of the cells exhibited different types of membrane protrusions. At this time point, an immunofluorescence assay was performed to visualize the subcellular distribution of SMN. As expected, in unstimulated fibroblasts, SMN displayed a punctuate pattern distributed throughout the whole cell body, and a typical localization in nuclear bodies, named gems (Fig. 1A, unstimulated). Surprisingly, in ATP-recovering cells, we observed a strong redistribution of SMN in vesicle-like structures within the protrusive areas of the plasma membrane. Interestingly, SMN-positive dots were also detectable along the cell perimeter of stimulated cells (Fig. 1A,B, stimulated). In order to correlate SMN distribution to the actin filament meshwork, we probed cells with phalloidin (Fig. 1C). Stimulated fibroblasts displayed a well-organized cortical actin network underneath the plasma membrane, as well as several filopodial extensions. In these cells, SMN accumulated at the tips of both the cortical actin arc and filopodia. Notably, in similar membrane protrusions observed in unstimulated fibroblasts, SMN was not detectable (see detail in Fig. 1C), suggesting that the peripheral recruitment or localization of SMN is mainly governed in an activity-dependent context. In support of this, and to exclude exacerbated effects due to the ATP depletion and recovery treatment, we tested the localization of SMN upon more physiological conditions known to induce actin filament rearrangements (Ridley, 2011). In particular, we performed immunofluorescence assays of starved fibroblasts stimulated with fetal bovine serum (FBS) for 30 min, or with basic fibroblast growth factor (bFGF, 50 ng/ml) for 15 min. Both conditions led to extension of cellular protrusions, although with a lesser frequency compared to the ATP depletion and recovery assay. However, in cells exhibiting membrane remodelling, we observed a peripheral accumulation of the SMN protein (see Fig. S1A), consistent with the idea that a fraction of SMN moves to the periphery in an activity-dependent manner. Given that accumulation of SMN at the raffling membrane could occur for a thickness effect, we examined the SMN distribution in fibroblasts expressing a freely diffusible green fluorescent protein (GFP). Following ATP depletion and recovery, we observed that GFP was present at the membrane protrusions, but it was not able to compensate for SMN recruitment at the same subregions (Fig. S1B). Finally, we also verified the subcellular distribution of another RNA-related protein. We checked the localization of KSRP, given that this RNA-binding protein interacts with SMN (Tadesse et al., 2008), and shuttles between nuclear and cytoplasmic compartments. In contrast to SMN, KSRP was not enriched in membrane protrusions, and its localization was almost unaffected in stimulated cells (see Fig. S1C).

Interestingly, these findings reveal a peripheral recruitment of SMN in structures underlying actin filament remodelling.

A fraction of SMN colocalizes with translation machinery at membrane protrusions

We asked whether molecules related to translational control were present in the same subregions where SMN was shown. In particular, we imaged cells for both RNA and components of translation machinery (Fig. 2A). Cellular RNA, including mRNPs, was labelled by using an RNA-selective fluorescent probe. In parallel, protein synthesis machinery was visualized by the immunostaining of ribosomal protein S6 (S6, also known as RPS6). In the case of RNA, in unstimulated cells, maximal fluorescence was detectable in the nucleoli and throughout the nucleus. A diffuse and faint signal was also present in the cytoplasmic compartment. Under the same conditions, the ribosomal protein S6 displayed a typical pattern throughout the cytoplasm (Fig. 2A, unstimulated). In stimulated cells, we found an asymmetrical redistribution of both RNA and S6, with a robust detection of the respective signals at the membrane protrusions (Fig. 2A, stimulated). Finally, to verify the presence of initiation sites of protein synthesis, we checked the phosphorylation status of S6 by using an antibody against S6 phosphorylated at Ser235 or Ser236 (phospho-S6). Phospho-S6 immunostaining suggested that there was active translational hotspots at the leading edge of stimulated cells (Fig. 2A, stimulated). To validate this result, we carried out the surface sensing of translation technology (SUnSET) (Schmidt et al., 2009). Newly synthesized proteins were traced by puromycin incorporation and revealed by immunostaining with anti-puromycin antibody. As shown in Fig. 2B, in stimulated fibroblasts, newly synthesized

Journal of Cell Science (2016) 129, 804-816 doi:10.1242/jcs.176750

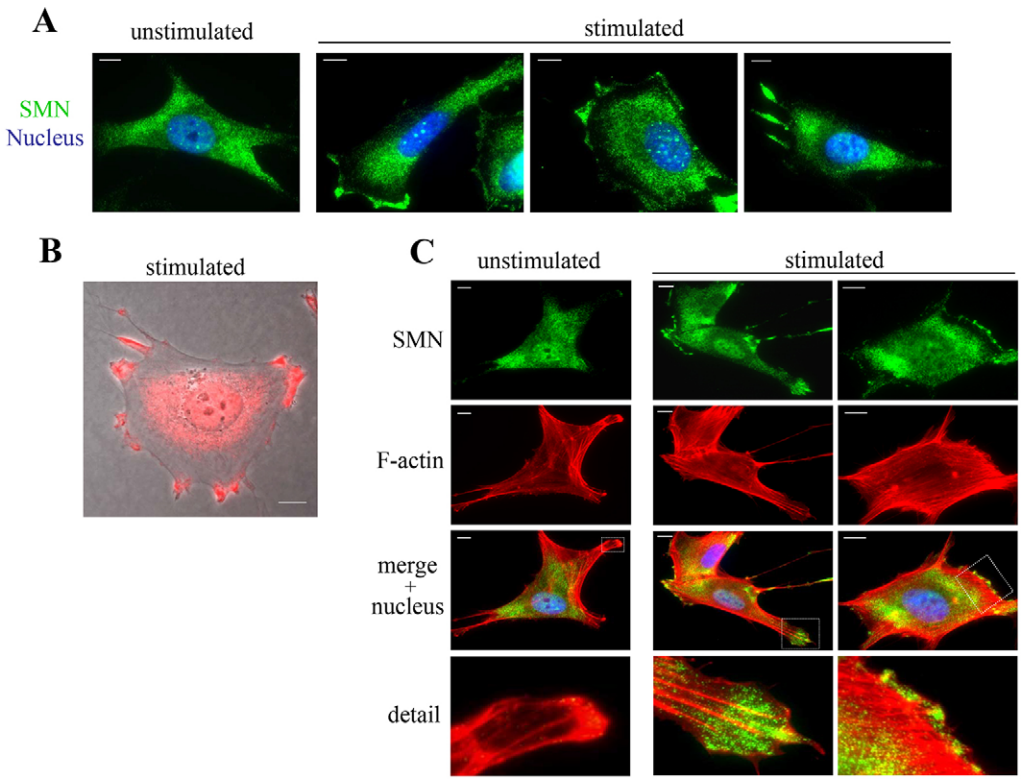

Fig. 1. SMN accumulates at membrane protrusions of ATP-recovering cells. (A–C) Representative fluorescence microscopy images. Human fibroblasts were untreated (unstimulated) or ATP-depleted for 60 min, and then stimulated to extend membrane protrusions by incubation in complete medium for 30 min (stimulated). Membrane protrusions were detectable in ∼70% of the stimulated cells. Cells were fixed and immunostained with anti-SMN antibody (green in A and C, red in B) or stained with Alexa-Fluor-594–phalloidin to visualize the F-actin filaments (C red). B shows a representative overlay of the phase contrast image with SMN immunostaining (red) of ATP-recovering cells (stimulated). The 'detail' images in C, represent high magnification images of the boxed area. Nuclei were labelled with DAPI (blue). Scale bars: 10 µm.

proteins were enriched at membrane protrusions, this pattern clearly overlapped with phospho-S6 as well as SMN immunostaining. Notably, the total fluorescence intensity of phospho-S6 was significantly stronger in fibroblasts extending protrusions (Fig. 2A,B, stimulated). This was consistent with a switching on of the mTOR pathway. We further monitored the mTOR pathway by western blot analysis. As shown in Fig. 2C, the p70S6 kinase, a downstream target of mTOR, shifted to an active status in fibroblasts extending protrusions, and this correlated with Ser235 or Ser236 phosphorylation in the S6 protein. This result was not surprising, because a direct link between mTOR activity and actin dynamics is a well-accepted notion (Berven et al., 2004; Hoeffer and Klann, 2010). Our main interest was to verify the colocalization between SMN and translation machinery during the actin remodelling. To this end, we subjected stimulated cells to dual immunofluorescence for SMN and S6, or SMN and phospho-S6, and then analysed slides by confocal laser scanning microscopy (Fig. 2D). Immunostaining of both SMN and the S6 proteins appeared to be overlapping in several subcellular regions. By performing *z*-stack imaging and orthogonal analysis, we identified several yellow dots that showed colocalization between SMN and both S6 and phospho-S6. Interestingly, the colocalization spots were preferentially located near the cell surface of stimulated cells (see graphs in Fig. 2D).

These data show that SMN partially compartmentalizes with translation machinery in cellular structures in which dynamic changes of the actin cytoskeleton are coupled with spatially restricted protein synthesis.

SMN associates with the plasma membrane

Taking into account our images displaying SMN dots along the cell perimeter of ATP-recovering cells (Fig. 1B), we suspected a physical contact of SMN with the plasma membrane. In order to support this hypothesis, we prepared plasma-membrane-enriched fractions from both unstimulated and ATP-recovering fibroblasts, and performed western blot analysis to check for SMN presence. As shown in Fig. 3A, SMN was detectable in plasma membrane fractions of both control (unstimulated) and ATP-recovering fibroblasts (stimulated), without significant differences. This result was apparently in disagreement with images showing the increased peripheral localization of SMN under stimulating conditions. We suppose that during actin remodelling, cytoplasmic SMN granules accumulate within membrane protrusions that are in close proximity, but not physically anchored, to the plasma membrane. In addition, a membrane-bound fraction of SMN, as revealed by the biochemical approach, is usually present, even if apparently it is less detectable by immunofluorescence assays. When we probed blots with an antibody specific for the core-splicing factor protein SmB (also known as SNRPB), only the whole-cell extracts displayed immunoreactive bands (Fig. 3A). This is consistent with the fact that the canonical SMN complex assembles Sm proteins into the cytoplasm (Li et al., 2014). We also tested components of the translation machinery. We used antibodies against S6 and L7 (also known as RPL7), markers of 40S and 60S ribosomal subunits, respectively. Both S6 and L7 were present in plasma membrane fractions from unstimulated fibroblasts (Fig. 3A). In contrast to SMN, no, or almost no, ribosomal proteins were detectable in plasma membrane fractions from stimulated cells. Interestingly, this result was in agreement with the previously published work (Tcherkezian et al., 2010) reporting that inactive ribosomes, anchored to plasma membrane of unstimulated neurons, are released in an activity-dependent manner. Notably, the endoplasmic reticulum (ER) marker, calreticulin, was present but not enriched in our plasma membrane preparations (Fig. 3A). In addition to fibroblasts, we also achieved similar results in HeLa cells. In western blot analyses, we observed a decrease of S6 in the plasma membrane fractions from both ATP-recovering and EGF-stimulated cells (see Fig. S2). This event correlated with Thr389

Journal of Cell Science (2016) 129, 804-816 doi:10.1242/jcs.176750

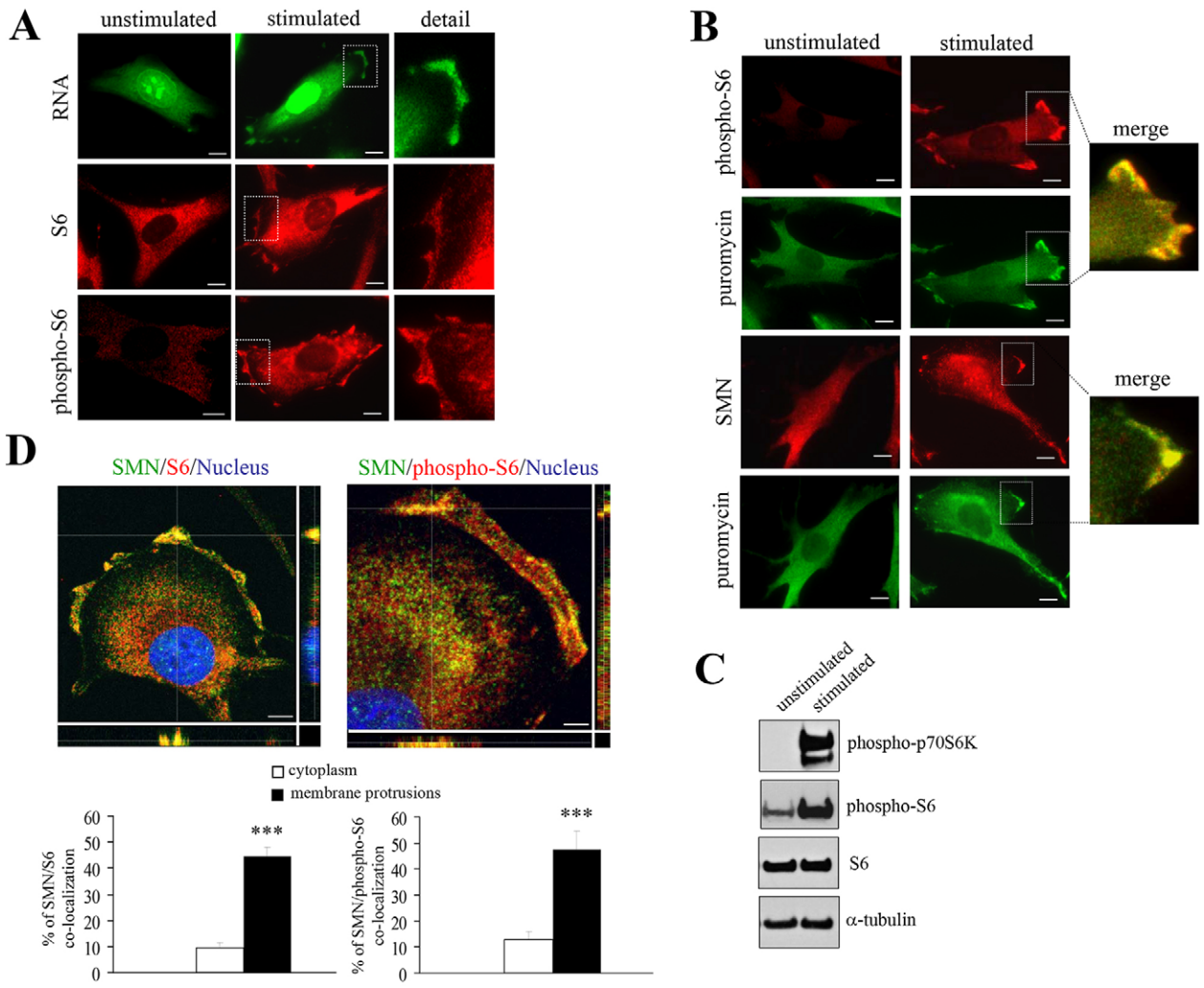

Fig. 2. SMN colocalizes with translation machinery in membrane protrusions. (A) Representative images of unstimulated and stimulated fibroblasts. Fixed cells were stained with SYTO RNAselect (green) or immunostained for S6 and phospho-S6 (Ser235 or Ser236) (red). The 'detail' images show a high magnification view of the boxed area of each panel. Scale bars: 10 µm. (B) Unstimulated and ATP-recovering fibroblasts (stimulated) were subjected to dual immunostaining for phospho-S6 (red), SMN (red) and puromycin (green). The high magnification panel shows the overlap in staining for the boxed areas. Scale bars: 10 µm. (C) A western blot analysis was performed in parallel for the cells described in A and B. Equal amounts of the protein extracts were analysed by using anti-phospho-p70S6K (Thr389) and anti-phospho-S6 antibodies. α-tubulin and S6 were monitored as controls of the protein loading. (D) Upper panels, representative confocal microscopy images of stimulated cells subjected to dual immunostaining with anti-SMN (green) and anti-S6 (red), or anti-SMN (green) and anti-phospho-S6 (red) antibodies. The nucleus is stained with DAPI (blue). Orthogonal projection of the confocal *z*-stack analysis showing colocalization (yellow) of SMN with both S6 and phospho-S6 at membrane protrusions. Scale bars: 10 µm (S6) 7.5 µm (phospho-S6). (D) Lower panels, quantification of SMN–S6 and SMN–phospho-S6 colocalization over the membrane protrusion and cytoplasm. Results are mean±s.e.m. (*n*=4). ***P<0.01 (unpaired t-test).

phosphorylation in p70S6 kinase, confirming that ribosomes are released from the plasma membrane in combination with mTOR switch-on. Likewise in fibroblasts, the amount of SMN anchored to plasma membrane fractions of HeLa cells appeared to be almost unchanged. This result not only excluded the possibility of a cell-type-specific event, but pointed to the idea that a translational platform anchored to the plasma membrane might occur commonly in many cell types. Furthermore, we carried out a more stringent fractionation approach to dissect membranes in different subdomains (Fig. 3B). Detergent-resistant membranes (DRMs), containing lipid rafts, can be separated from heavy non-raft domains and analysed by western blot assay. In both unstimulated and ATP-recovering fibroblasts (stimulated), the majority of SMN protein was detectable in the non-raft fractions of membranes. However, SMN was also present in lipid-raft-containing light fractions. Interestingly, the amount of raft-localized SMN protein increased following the cellular ATP-recovery treatment (Fig. 3B, stimulated). Apparently, L7 was not recovered in DRMs. Given that detergent extraction affects lipid–protein interactions, so that only the proteins strongly associated with lipids are detectable in DRMs (Schuck et al., 2003), we could not exclude the presence of ribosomal proteins also in lipid rafts subdomains.

Collectively, we provide biochemical evidence of a physical association of SMN with plasma membrane. In addition, these data suggest that SMN protein relocalizes at specific plasma membrane subdomains during actin or cell surface remodelling.

SMN interacts with caveolin-1

To further define the SMN–membrane association, we verified a possible interaction between SMN and caveolin-1. Caveolin-1 is the main component of plasma membrane caveolae, which are implicated in cell membrane composition and expansion, and cytoskeleton

Journal of Cell Science (2016) 129, 804-816 doi:10.1242/jcs.176750

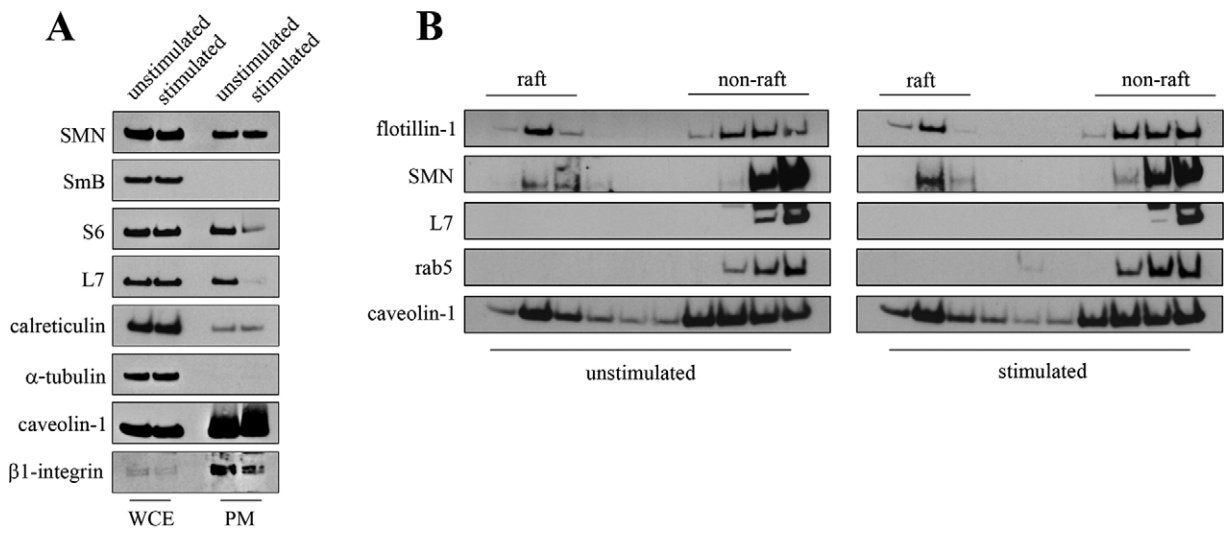

Fig. 3. SMN–plasma-membrane association. (A) Representative western blot analysis of whole-cell extracts (WCE) and plasma-membrane-enriched fractions (PM), from unstimulated and ATP-recovering cells (stimulated). Equal amounts of the protein extracts were immunoblotted for SMN and SmB. The anti-S6 and -L7 antibodies were used to monitor the 40S and 60S ribosomal subunits, respectively. α-tubulin was detected as cytoplasmic marker. Calreticulin was checked as the ER marker. Both caveolin-1 and β1-integrin were detected as plasma membrane markers. (B) Raft and non-raft membrane subdomains were isolated from both unstimulated and ATP-recovering (stimulated) fibroblasts. Cell lysates were solubilized with 20 mM CHAPS and subjected to sucrose density gradient centrifugation. A total of ten fractions, collected from the top of each gradient, were analysed by western blotting. Lipid-raft-containing light fractions were revealed by the specific markers flotillin-1 and caveolin-1. Rab5 was used as marker of heavy non-raft fractions. Blots are representative of three independent experiments.

remodelling (Grande-García et al., 2007; Dubroca et al., 2007). Furthermore, we were very interested to explore a possible link between caveolin-1 and SMN, because caveolin-1 unexpectedly appears in the interaction map of modifier genes of SMN defects (Dimitriadi et al., 2010). To this end, we prepared plasma membrane fractions from unstimulated fibroblasts, and carried out co-immunoprecipitation assays by using anti-caveolin-1 antibody. SMN co-precipitated with caveolin-1 from the plasma membrane fractions, which also displayed immunoreactivity to the anti-L7 antibody (Fig. 4A, left). This result was confirmed by reciprocal co-immunoprecipitation using a monoclonal antibody against SMN (Fig. 4A, right). These findings provided biochemical evidence that SMN coexists with components of translation machinery in caveolin-rich membrane domains. In parallel, we imaged cells subjected to dual immunostaining for SMN and caveolin-1. Interestingly, colocalization spots were seen in both intracellular and peripheral subregions (see Fig. S3A). SMN–caveolin-1 association was also explored by an *in situ* proximity ligation assay (PLA), which reveals endogenous protein–protein interactions in fixed cells. Both unstimulated and ATP-recovering fibroblasts were subjected to PLA using antibodies against SMN and caveolin-1, and then processed for confocal microscopy (Fig. 4B,C). In unstimulated cells, several PLA dots were present, and some of these dots were clearly detectable at the cellular leading edge (Fig. 4B). Interestingly, PLA occurrence was significantly increased in ATP-recovering fibroblasts (Fig. 4C). PLA specificity was validated by testing different combinations of primary antibodies against SMN and caveolin-1 (see Fig. S3B). By performing *in situ* PLA, we confirmed that the interaction between SMN and caveolin-1 also occurs in cultured neurons from rat spinal cord (see Fig. S3C). PLA was performed in untreated or brain-derived neurotrophic factor (BDNF)-stimulated spinal cord neurons. Notably, BDNF treatment led to higher PLA signals, compared to the unstimulated cultures. These data prompted us to investigate whether caveolin-1 could affect SMN and/or ribosome linkage at the plasma membrane. We assessed this aspect by preparing plasma membrane fractions from caveolin-1-depleted fibroblasts (Fig. 4D). Fibroblasts transfected with control small interfering RNA (siRNA) (siC) or siRNA against caveolin-1 (siCav-1) were subjected to the ATP depletion and recovery assay, and then processed to obtain plasma membrane fractions. Western blot analysis showed that caveolin-1 deficiency did not change the SMN abundance at the plasma membrane of unstimulated cells. More substantial differences were observed in plasma membrane fractions from ATP-recovering cells (stimulated), which retained more SMN protein following caveolin-1 knockdown. Interestingly, caveolin-1 deficiency depleted plasma membrane compartments of ribosomal proteins (Fig. 4D).

These results suggest that SMN could contact the plasma membrane in a caveolin-1-independent manner. However, caveolin-1 could affect turn over of membrane SMN. In addition, we provide evidence that caveolin-1 could mediate ribosome anchoring.

SMN depletion impairs actin dynamics

By performing loss of function studies, we evaluated the effects of SMN function in actin dynamics. We reduced the expression of endogenous SMN by the transient transfection of fibroblasts with *SMN1*-selective siRNAs (siSMN). Scrambled siRNAs were used as control (siC). At 48 h post transfection, we probed actin filaments and imaged cells by using fluorescence microscopy (Fig. 5A). Unstimulated cells displayed mild perturbations of the actin meshwork in the absence of SMN (Fig. 5A, unstimulated). Major differences were observed under stimulating conditions (Fig. 5A, stimulated). In particular, stimulated control cells were able to properly reassemble actin filaments, exhibiting robust actin arcs, as well as several filopodial extensions. Under the same condition, SMN-depleted cells displayed an aberrant and unorganized actin network. In the absence of SMN, the amount of actin filaments in the growing tips of filopodia appeared to be low compared to similar structures observed in control cells (Fig. 5A′). Overall, the ability to extend membrane protrusions was significantly reduced in SMN-deficient fibroblasts (Fig. 5B). Moreover, owing to the non-oriented cytoskeleton, we thought that SMN-depleted cells were unable to deliver mRNPs for local translation. To verify this idea, we assessed

Journal of Cell Science (2016) 129, 804-816 doi:10.1242/jcs.176750

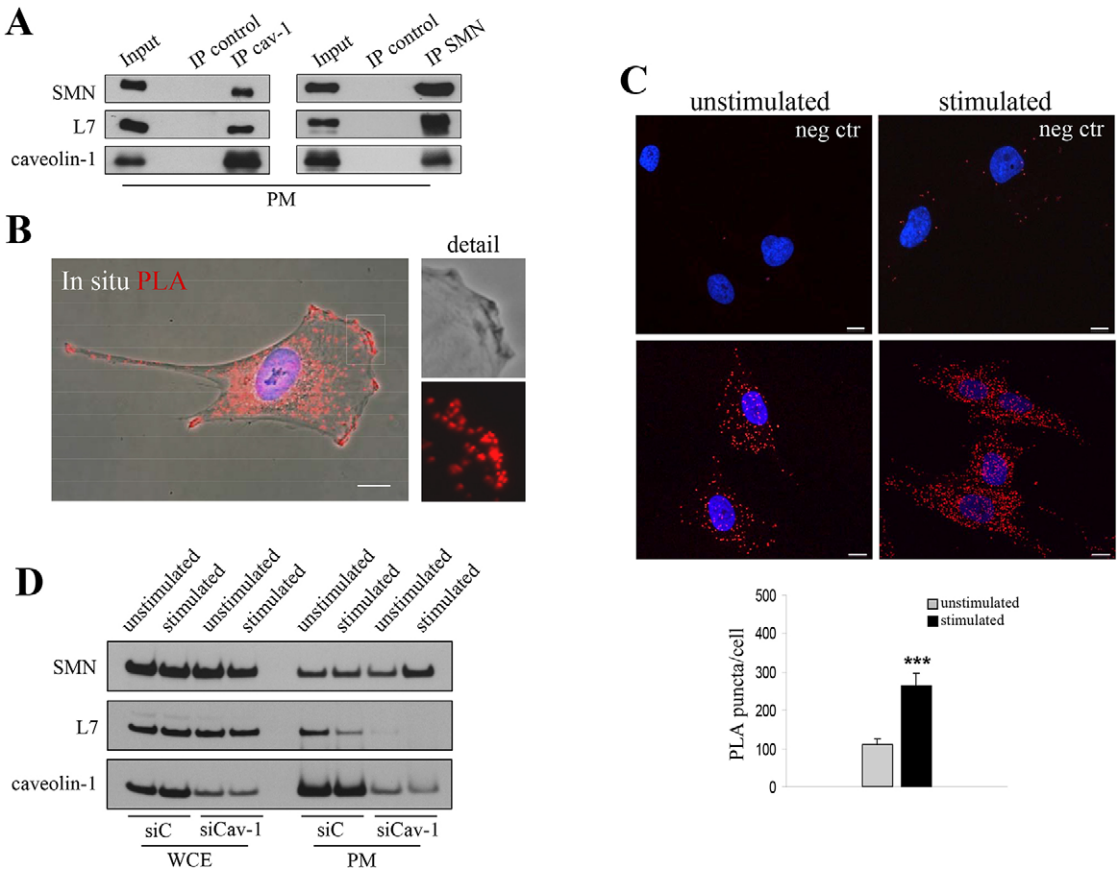

Fig. 4. SMN interacts with caveolin-1. (A) Plasma-membrane-enriched fractions (PM) from untreated fibroblasts were immunoprecipitated with non-specific antibodies (immunoprecipitation control), anti-caveolin-1 polyclonal antibody (IP cav-1) or anti-SMN monoclonal antibody (IP SMN). 10% of the total lysates was used as input. Antibodies against SMN, L7, and caveolin-1 were used for the western blot analysis. (B) An *in situ* proximity ligation assay (PLA) was performed in unstimulated fibroblasts using primary antibodies against SMN and caveolin-1 [polyclonal (Santa Cruz Biotechnology) and monoclonal (R&D), respectively]. The representative overlay of phase-contrast and PLA images (red dots) was obtained by epifluorescence microscopy. The 'detail' image represents a high magnification of the boxed area. Nuclei were stained with DAPI (blue). Scale bar: 10 µm. (C) The PLA assay was performed on both unstimulated and ATP-recovering fibroblasts (stimulated) using primary antibodies against SMN and caveolin-1 [monoclonal (BD) and polyclonal (Santa Cruz Biotechnology), respectively]. Detection of PLA signals (red dots) was achieved by confocal microscopy. As a negative control, one of the primary antibodies was omitted (neg ctr). Nuclei were stained with DAPI (blue). Scale bars: 10 µm. The graph shows a quantification of PLA puncta per cell indicating the increased SMN–caveolin-1 interaction in ATP-recovering cells (stimulated). Data are the mean from three independent experiments. Results are mean±s.e.m. (n=4). ***P<0.01 (unpaired t-test). (D) Western blot analysis of both whole-cell extracts (WCE) and plasma-membrane-enriched fractions (PM) from fibroblasts transfected with control (siC) or caveolin-1 siRNA (siCav-1), and subjected to an ATP-depletion and recovery assay. The density of the immunoreactive bands to anti-caveolin-1 antibody were reduced in caveolin-1-deficient-cells. Immunoblots are representative of three independent experiments.

the subcellular localization of β-actin mRNA. We focused on the β-actin transcript for two main reasons: (1) the β-actin mRNA asymmetrically relocalizes in regions where actin protein production supports cell polarity, and (2) its peripheral distribution has been linked to SMN function. To visualize both β-actin transcript and the SMN protein, fibroblasts extending protrusions were subjected to combined fluorescent *in situ* hybridization (FISH) and immunostaining. As showed in Fig. 5C, in the absence of SMN, β-actin mRNA appeared diffuse throughout the cytoplasm, without asymmetrical accumulation to the cell periphery. The quantification of the FISH signal confirmed the reduced peripheral recruitment of β-actin transcript in SMN-depleted cells (Fig. 5D). These results strongly confirm the notion that SMN loss of function is deleterious in actin-based membrane remodelling.

SMN loss of function depletes the plasma membrane of ribosomes

It has been reported that dysregulated mTOR signalling occurs in the SMA disease context (Kye et al., 2014). This prompted us to verify whether, in our SMN-depleted cells, the perturbation of actin network combines with a reduced mTOR activity. Western blot analysis of fibroblasts stimulated to extend protrusions revealed that the p70S6 kinase was activated in both control and SMN-depleted cells (Fig. 6A). Phospho-S6 immunostaining confirmed that mTOR and p70S6 activity was independent of SMN expression levels (see Fig. S4A). Notably, in stimulated SMN-knockdown cells, phospho-S6 immunostaining appeared diffuse throughout the cytoplasm, without peripheral accumulations. Apparently, our findings are in disagreement with the notion that SMN deficiency dysregulates mTOR activity (Kye et al., 2014). However, we do not exclude perturbed translational events downstream of mTOR. To assess this question, we evaluated *in vivo* the protein synthesis rate of SMN-depleted cells by performing a SUnSET assay. Both siC- and siSMN-transfected fibroblasts were subjected to ATP depletion and recovery assay, in which the ATP recovery step was carried out in the presence or absence of the mTOR inhibitor rapamycin. Newly synthesized proteins were traced by puromycin incorporation and detected by western blot analysis with anti-puromycin antibody

Journal of Cell Science (2016) 129, 804-816 doi:10.1242/jcs.176750

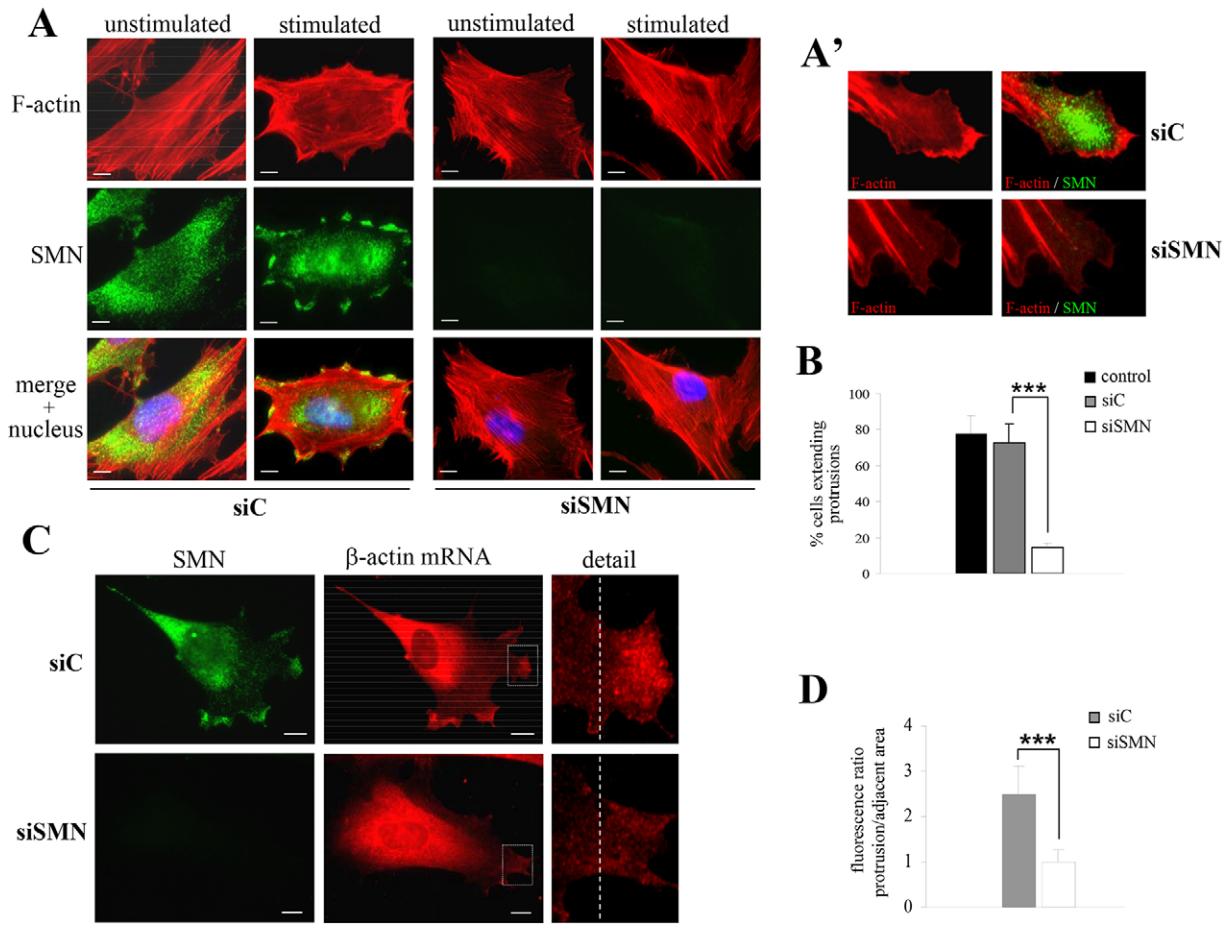

Fig. 5. SMN depletion affects actin filaments assembly. (A) Representative images of fibroblasts transfected with the control (siC) or *SMN1* siRNA (siSMN). Unstimulated and stimulated cells were immunostained for SMN (green) or probed for F-actin (red). Nuclei were counterstained with DAPI (blue). Scale bars: 10 µm. (A′) Representative images of filopodial structures, observed in both stimulated control cells (siC) and SMN-depleted cells (siSMN). (B) Graph showing the percentage of the cells extending protrusions, for each of the untransfected (control), siC and siSMN groups. Data are the mean± s.e.m. from four independent experiments, in which a total of 50 cells were analysed for each group. ***P<0.01 (unpaired t-test). (C) Fibroblasts extending protrusions were subjected to combined FISH and immunostaining. The localization of the SMN protein (green) and β-actin mRNA (red) was visualized by performing fluorescence microscope. The 'detail' image represents a high magnification of the boxed area. Scale bars: 10 µm. (D) Graph showing the increase of β-actin mRNA in the protrusions of both siC- and siSMN-stimulated cells. The fluorescence signal from each protrusion was normalized to signal from the adjacent area (left region delimited by the dashed line). Data are the mean±s.e.m. from three independent experiments in which a total of 25 membrane protrusions was analysed for each experimental group. ***P<0.01 (unpaired t-test).

(Fig. 6B). In non-stimulating conditions, no significant differences were observed in the protein synthesis efficiency following SMN depletion. In stimulated cells, SMN knockdown resulted in an ∼25% reduction of translation. This difference was completely abolished by rapamycin treatment, suggesting that a subset of protein synthesis, downstream of mTOR, could depend on SMN function. As shown above, the plasma membrane of unstimulated fibroblasts exhibited immunoreactivity to SMN as well as ribosomal components of translation machinery (Fig. 3A). Next, therefore, we asked whether SMN could be implicated in the ribosome–membrane association. To this end, we performed western blot analysis of plasma membrane fractions from transiently SMN-depleted fibroblasts (Fig. 6C). In the absence of SMN, the ribosomal proteins were not detectable in plasma membrane compartments, although their total expression remained unchanged (Fig. 6A). This could be explained by an exacerbated activation of mTOR pathway. We excluded this because, in our system, SMN depletion was not sufficient to activate the signalling cascade downstream of mTOR (Fig. 6A). Moreover, we isolated DRMs fractions from unstimulated siC- and siSMN-transfected fibroblasts. By using western blot analyses, we showed that SMN deficiency changed the membrane distribution of both L7 and caveolin-1. In particular, the abundance of caveolin-1 was mainly reduced at the DRMs (Fig. 6D). These results suggest that SMN can affect the protein composition of the plasma membrane and highlight a possible involvement of SMN in assembly of ribosomal proteins into caveolin-1-rich membranes. In order to exclude a cell culture artefact, we also addressed the main crucial aspects of this study in a SMA pathological background. We prepared plasma membrane fractions from primary fibroblasts of both a severe type I SMA patient and an unaffected individual. By western blot analysis, we found that the SMA condition reduces the amount of ribosomes in plasma membrane compartments (Fig. 7A). In these cells, we also tested DRM fractions, confirming similar results obtained in transfected fibroblasts (Fig. S4B). Furthermore, by performing a western blot analysis, we showed that the ATP recovery treatment switched on mTOR activity to a similar degree in unaffected and SMA-affected fibroblasts (Fig. 7B). However, protein synthesis rate downstream of mTOR activation (stimulated) was reduced in SMA fibroblasts by ∼25%, as evaluated by the SUnSET assay (Fig. 7C). No significant differences were observed in

Journal of Cell Science (2016) 129, 804-816 doi:10.1242/jcs.176750

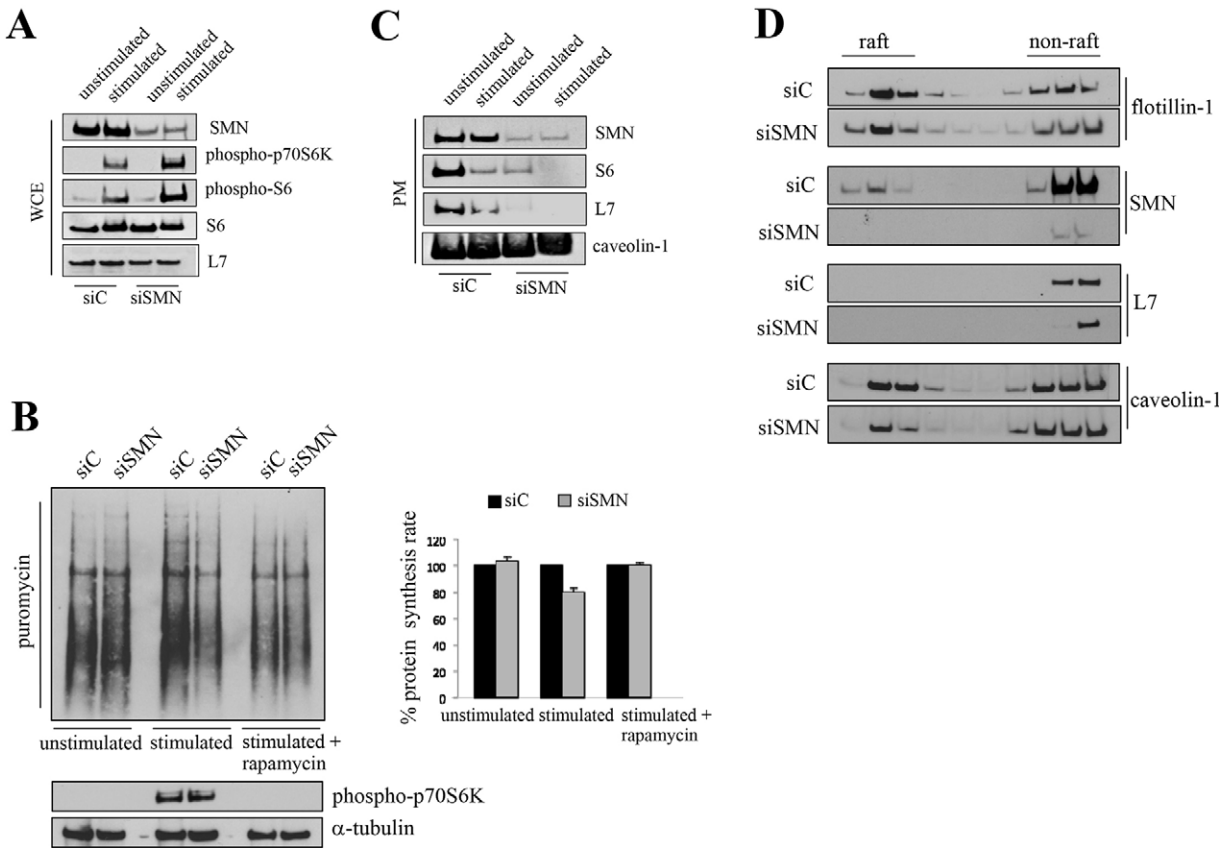

Fig. 6. SMN loss of function depletes membranes of ribosomes. (A) Western blot analysis of siC- and siSMN-transfected fibroblasts, stimulated or not to extend membrane protrusions by an ATP depletion and recovery assay. Equal amounts of the whole-cell extracts (WCE) were tested for phospho-p70S6K (Thr389) and phospho-S6 (Ser235 or Ser236). The total pool of both S6 and L7 was detected. (B) Evaluation of protein synthesis rate by SUnSET. Both siC- and siSMN-transfected fibroblasts were subjected to an ATP depletion and recovery assay, in the presence or absence of rapamycin. Equal amounts of the protein extracts were immunoblotted and analysed using anti-puromycin. Phospho-p70S6K (Thr389) was monitored as a control for the rapamycin effect. α-tubulin was detected as a protein-loading control. The graph shows a quantification of protein synthesis rate of SMN-depleted fibroblasts (siSMN) compared to control cells (siC), expressed as percentage. Data are the mean±s.e.m. from three independent experiments. (C) Western blot analysis of plasma-membrane-enriched fractions (PM) from siC- and siSMN-transfected fibroblasts subjected to an ATP depletion and recovery assay. Equal amounts of proteins were immunoblotted for the indicated antibodies. (D) siC- and siSMN-transfected fibroblasts, subjected to an ATP depletion and recovery assay, were processed to isolate raft and non-raft fractions. The indicated antibodies were used for immunoblot analysis. Blots are representative of three independent experiments.

unstimulated conditions. Finally, we also subjected the SMA fibroblasts to an ATP depletion and recovery assay in order to test their ability to undergo actin cytoskeleton remodelling. By probing the actin network with phalloidin, we observed that SMA fibroblasts failed to rearrange actin filaments in stimulating conditions (Fig. 7D, stimulated). This was clearly evident by defective lamellipodia formation and irregular filopodial protrusions. As expected, in non-stimulating conditions, SMN deficiency impacted on cytoskeleton organization to a lesser extent (Fig. 7D, unstimulated). The results obtained in SMA patient fibroblasts confirm the idea that SMN is involved in membrane sequestering of ribosomes, and recapitulate main crucial aspects observed in transfected SMN-depleted cells.

DISCUSSION

It is still unclear why motoneurons, more than any other cell type, need high levels of SMN protein for their survival. Taking into account the housekeeping role of SMN in RNA metabolism, the idea is that SMN expression levels could become crucial depending on the phenotypic context in which this protein operates. Two peculiarities of motoneurons are of particular interest: (1) the large extension and polarity, and (2) the neuromuscular junction (NMJ), a specialized membrane domain, which physically and functionally interconnects the motoneuron to muscle. Both these features are structurally governed by dynamic rearrangements of actin filament, which in turn require local protein synthesis of key regulatory factors. Consistent with the above hypothesis, the interaction map of SMA modifier genes identifies three specific pathways in which SMN can act: actin remodelling, local translational control and endocytosis (Dimitriadi et al., 2010). Of note, membrane signalling dictates each of these pathways, and their crosstalk drives the establishment of cell polarity. This scenario suggests a new context in which SMN can work, and raises some important questions: can SMN mediate the functional interplay of cellular pathways specified by SMA modifier genes? Can an exacerbated cell polarity represent the ‘Achilles’ heel’ for SMN-depleted cells? Moreover, and most importantly: how could SMN, an RNA regulatory protein, interconnect membrane signalling and the actin network? To investigate *in vitro* some of these aspects, we took advantage of an ATP depletion and recovery assay. This method, based on the action of metabolic inhibitors on the actin cytoskeleton, stimulates and recapitulates typical changes of actin filament underlying the establishment of cell polarity (Svitkina et al., 1986). For this specific issue and approach, the fibroblast is the best-performing cell.

Journal of Cell Science (2016) 129, 804-816 doi:10.1242/jcs.176750

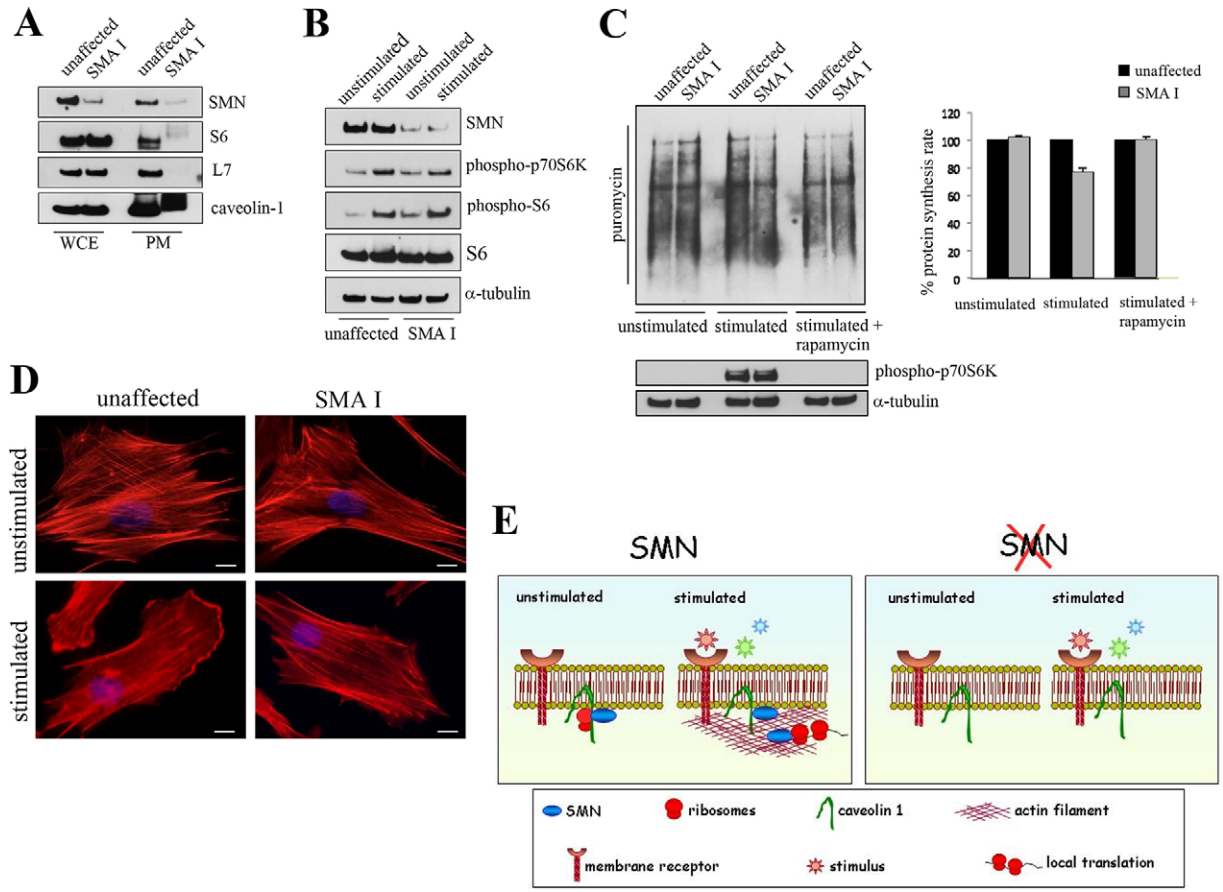

Fig. 7. SMA type I fibroblasts. (A) Western blot analysis of whole-cell extracts (WCE) and plasma-membrane-enriched fractions (PM) from unaffected and SMA type I fibroblasts. Equal amount of proteins were immunoblotted for SMN. The S6 and L7 protein were tested as ribosomal markers. The quality of plasma membrane fractions was controlled by monitoring caveolin-1. (B) Western blot analysis of unaffected and SMA type I fibroblasts, stimulated or not to extend protrusions. Equal amounts of the whole-cell extracts were tested for phospho-p70S6K (Thr389) and phospho-S6 (Ser235 or Ser236). α-tubulin and S6 were monitored as controls of protein loading. (C) Evaluation of protein synthesis rate by SUnSET. Fibroblasts from an unaffected individual (unaffected) and those from a SMA type I patient (SMA I) were subjected to an ATP depletion and recovery assay, in the presence or absence of rapamycin. Equal amounts of the protein extracts were immunoblotted and analysed using anti-puromycin antibody. Phospho-p70S6K (Thr389) was monitored to control the rapamycin effect. α-tubulin was detected as a protein-loading control. Puromycin incorporation was quantified by densitometric analysis of the corresponding immunoblots, normalized to α-tubulin. The graph shows a quantification of the protein synthesis rate of the SMA type I fibroblasts compared to control unaffected cells expressed as percentage. Data are the mean±s.e.m. from three independent experiments. (D) Representative fluorescence microscope images. Fibroblasts from the unaffected individual and SMA type I patient were unstimulated or stimulated to extend protrusions in the ATP depletion and recovery assay, and probed for F-actin (red). DAPI was used to label nuclei (blue). Scale bars: 10 µm. (E) Schematic representation for the mechanism by which SMN couples activity-dependent local translation to actin remodelling. SMN mediates the anchoring of an inactive pull of ribosomes to caveolin-rich membrane domains. Under appropriate cues, ribosomes are released from the plasma membrane and rapidly engaged into actively translating polyribosomes. This event underlies dynamic rearrangements of actin cytoskeleton. SMN loss of function depletes the plasma membrane of inactive ribosomes, and this renders plasma membrane not competent to govern the activity-dependent local production of factors implicated in actin and membrane remodelling.

In our experience, checking for subcellular distributions of a protein during a specific event can help researchers to understand its function. Previous attempts to map the intracellular localization of SMN have revealed that this protein is mainly present in the nucleus and perinuclear cytoplasm of all cell types. This localization has been linked to the canonical role of SMN in snRNPs biogenesis. However, the presence of SMN granules in subcellular regions, such as the axonal growth cone, filopodia-like structures and the NMJ (Fan and Simard, 2002; Fallini et al., 2012; Dombert et al., 2014), implies an involvement of SMN beyond snRNP assembly. Here, we provide evidence in line with this assumption. First, when we stimulate fibroblasts to reassemble the actin cytoskeleton, SMN appears to be strongly redistributed at the cell protrusions, where the biogenesis of actin network begins (Svitkina et al., 1986). Both components of translation machinery and newly synthesized proteins are present at the same substructures. Indeed, it has been already reported that foci of active protein synthesis are present at the leading edge of fibroblasts during migration (Willett et al., 2013). This suggests that the molecular context in which the SMN function takes place might be related to local translational control. In more detail, colocalization studies show that SMN contacts the translational hotspots underlying membrane remodelling. A colocalization between SMN and polyribosomes has been previously reported (Béchade et al., 1999). However, in that study a direct link to actin dynamics was not proposed. Next, SMN relocalizes to membrane protrusions in a cellular context in which the mTOR–p70S6K signalling cascade couples to actin remodelling. Regarding SMN localization, we also obtained similar results in fibroblasts stimulated with serum or bFGF. These findings highlight two important unique functions of SMN: (1) that cell surface remodelling combines with changes in cytoplasmic distributions of SMN, and (ii) that SMN accumulates at the cell

Journal of Cell Science (2016) 129, 804-816 doi:10.1242/jcs.176750

periphery in an activity-dependent manner. In this framework, receptor tyrosine kinases (RTKs) could be a triggering component for SMN trafficking, given that actin dynamics require RTK activation. Further studies will focus on this aspect.

Surprisingly, more than a signalling-dependence for SMN distributions, here we found a physical link between SMN and the plasma membrane. Immunofluorescence images support SMN–membrane linkage mostly in stimulated cells, in which the cytoskeleton organization unmasks SMN dots along the cell perimeter. Biochemical approaches reveal that SMN is always detectable in plasma-membrane-enriched fractions from fibroblasts, independently of their activity to extend membrane protrusions. In more detail, by performing DRM isolation, we observed that SMN is partially associated with lipid-raft-containing fractions, which retain more SMN protein following ATP recovery treatment. The notion that SMN associates with lipid rafts could be coherent with published works suggesting a link between lipid rafts and translational control. In particular, the netrin receptor DCC, which anchors protein synthesis machinery in neurons (Tcherkezian et al., 2010), partially localizes at lipid rafts and this association is required for axon outgrowth (Hérincs et al., 2005). Importantly, deficiency of the RNA-binding protein FMRP changes lipid rafts properties (Kalinowska et al., 2015). In contrast to SMN, ribosomal subunits are present only in plasma membrane preparations from unstimulated fibroblasts. In agreement with Flanagan and co-workers, we confirm that ribosomes are released from the membrane compartment in an activity-dependent manner (Tcherkezian et al., 2010). However, further studies are necessary to elucidate the connection between the SMN fraction that accumulates in close proximity to the plasma membrane and the SMN fraction found in direct association with it. In this regard, the demonstration of a bidirectional movement of fluorescently tagged SMN granules in the axon could be relevant (Zhang et al., 2003). Notably, these mobile SMN granules do not include core-splicing factor proteins. It will be interesting to assess whether the trafficking of these granules to and from the plasma membrane contributes to the rapid turnover of the membrane SMN. In this context, an important novelty of our study is that SMN associates with caveolin-1. Interestingly, cellular events triggering membrane expansions increase intracellular contacts between SMN and caveolin-1. It is of note that an intimate connection between SMN and caveolin-1 has already been suggested (Dimitriadi et al., 2010). Hart and colleagues observed that proteins related to endocytosis, including caveolin-1, unexpectedly predominate in the interaction map of SMN modifier genes. Consistent with this, defects in vesicle endocytosis and recycling have been observed at the NMJ in mice severely deficient for SMN (Kong et al., 2009). More investigations are needed to understand the functional and physical relationship between SMN and caveolin-1, as well as other factors, pertinent to endocytosis. Indeed, the interdependence of the mRNA translational control with the endocytosis pathway is still enigmatic. In this context, two of our results become attractive: (1) ribosomal proteins are sequestered like SMN in caveolin-1 enriched domains; and (2) caveolin-1 mediates anchoring of ribosomal proteins at the plasma membrane. By performing loss-of-function experiments, we found that SMN-depleted fibroblasts fail to rearrange F-actin and, consequently, to generate membrane protrusions. The non-oriented actin cytoskeleton, occurring in the absence of SMN, impairs the recruitment of β-actin transcripts at the leading edge of the cell. In this regard, we do not exclude that perturbations of β-actin-mRNA-binding proteins linked to the SMN fate might produce cumulative effects (Fallini et al., 2012). Next, in our system, SMN knockdown cells retain the ability to activate the mTOR pathway. Despite the mTOR pathway switch on, SMN loss of function reduces the protein synthesis rate by ∼25%. Of note, in non-stimulating conditions, the translational efficiency is almost unaffected by SMN loss of function. This result suggest a possible functional role for SMN in a subset of protein synthesis downstream of mTOR. Finally, a recent work has shown that localized mTOR-dependent protein synthesis is a prerequisite for the membrane expansion during axon outgrowth (Gracias et al., 2014). Given that SMN controls different tasks within RNA metabolism, the effect of its reduction could not only depend on SMN localization. However, this does not negate the role of SMN at the cell protrusions. Importantly, we show that SMN deficiency depletes the plasma membrane of ribosomes, and this correlates with the altered distribution of caveolin-1 at DRMs. Of note, this result was also confirmed in SMA-affected fibroblasts.

Collectively, our findings are compatible with a model in which SMN arranges the translational platform anchored to the plasma membrane, whose components are engaged for local protein synthesis underlying membrane remodelling (Fig. 7E). Future works should be planned to understand how SMN contributes to the packaging and/or delivery of membrane proteins competent for local translation. In addition, our study shows that a cytoplasmic pool of SMN colocalizes with S6 near the plasma membrane. It will be interesting to explore in what direction, from and/or to the plasma membrane, it occurs. This study opens a novel and exciting scenario in SMN investigations providing the opportunity not only to advance in functional characterization of the ubiquitous SMN protein, but also to understand how this new aspect of SMN might be crucial for motoneuron activity.

MATERIALS AND METHODS

Antibodies and reagents

The following antibodies were used: anti-SMN mouse monoclonal antibody (cat. no. 610647, BD Transduction Laboratories; work dilution for western blotting, 1:10,000; for immunofluorescence, 1:150); anti-SMN rabbit polyclonal antibody (cat. no. sc-15320, Santa Cruz Biotechnology; work dilution for immunofluorescence, 1:150); anti-S6 rabbit polyclonal antibody (cat. no. 2217, Cell Signaling Technology; work dilution for western blotting 1:1000; for immunofluorescence, 1:100); anti-phospho-S6 (Ser235 or Ser236) rabbit monoclonal antibody (cat. no. 4858, Cell Signaling Technology; work dilution for western blotting 1:1000; for immunofluorescence 1:100); anti-phospho-p70S6K (Thr389) rabbit polyclonal antibody (cat. no. 9234, Cell Signaling Technology; work dilution for western blotting 1:1000; for immunofluorescence, 1:100); anti-KSRP rabbit polyclonal antibody (cat. no. 5398, Cell Signaling Technology; work dilution for immunofluorescence, 1:100); anti-α-tubulin mouse monoclonal antibody (cat. no. T6074, Sigma-Aldrich; work dilution for western blotting, 1:2000); anti-flotillin-1 rabbit polyclonal antibody (cat. no. F1180, Sigma-Aldrich; work dilution for western blotting, 1:1000); anti-Caveolin-1 rabbit polyclonal antibody (cat. no. sc-894, Santa Cruz Biotechnology; work dilution for western blotting, 1:5000; for immunofluorescence, 1:200); anti-Caveolin-1 mouse monoclonal antibody (cat. no. MAB5736, R&D Systems; work dilution for immunofluorescence, 1:200); anti-Caveolin-1 monoclonal antibody (cat. no. NB100-615, Novus Biologicals; work dilution for immunofluorescence 1:200); anti-L7 rabbit monoclonal antibody (cat. no. ab 172478, Abcam; work dilution for western blotting, 1:1000); anti-Rab5 rabbit polyclonal antibody (cat. no. ab 18211, Abcam; work dilution for western blotting, 1:500); anti-digoxigenin sheep polyclonal antibody (cat. no. ab 64509, Abcam; work dilution for immunofluorescence 1:100); anti-puromycin mouse monoclonal antibody (cat. no. MABE343, Millipore; work dilution for western blotting, 1:25,000; for immunofluorescence, 1:10,000); and anti-calreticulin rabbit polyclonal antibody (cat. no. ADI-SPA-600, Stressgen Biotechnologies Corporation; work dilution for western blotting, 1:3000). The secondary antibodies conjugated to horseradish peroxidase were purchased from Jackson Immuno Research Laboratories and used at a dilution of 1:10,000. The

Journal of Cell Science (2016) 129, 804-816 doi:10.1242/jcs.176750

Alexa-Fluor-488 or Alexa-Fluor-594-conjugated secondary antibodies were purchased from Life Technologies and used at a dilution of 1:250. The anti-Sm mouse monoclonal antibody Y12, was a gift from Mauro Cozzolino (CNR, Institute of Translational Pharmacology, Italy). Anti-β1-integrin rabbit polyclonal antibody, was a gift from Rita Falcioni (Regina Elena Cancer Institute. Italy). The SytoRNASelect probe and Alexa-Fluor-594-conjugated phalloidin were from Life Technologies.

Cell cultures, treatments and transfections

hTert-immortalized human fibroblasts, obtained from Silvia Soddu (Regina Elena Cancer Institute. Italy) (Rinaldo et al., 2012), were cultured in Dulbecco's modified Eagle's medium (DMEM, Gibco) supplemented with heat inactivated 10% FBS (Gibco), penicillin-streptomycin (Gibco) and GlutaMAX (Gibco), in a 5% CO_2 humidified atmosphere, at 37°C. For serum stimulation, fibroblasts were cultured for 16 h in free-serum medium and then were incubated in presence of 15% fetal bovine serum for 30 min. For bFGF stimulation (Prepotech), starved fibroblasts were treated with bFGF (50 ng/ml) for 15 min. Human fibroblasts from the SMA type I patient (GM00232) and healthy control (GM08333) were obtained from the Coriell Institute for Medical Research (Camden, NJ, USA), and cultured in DMEM medium supplemented with 10% FBS, penicillin-streptomycin, and GlutaMAX, in 5% CO_2 humidified atmosphere, at 37°C. For EGF stimulation (Prepotech), starved HeLa cells were treated with EGF (50 ng/ml) for 5 min. For knockdown experiments, cells were transfected with a combination of three siRNA-27 duplexes targeting the human *SMN1* gene or the human caveolin-1 gene. Universal scrambled siRNA duplex was used as negative control (OriGene). For GFP transfection experiments, hTert-immortalized human fibroblasts were transfected with pEGFP plasmid (Clontech). Lipofectamine 2000 (Life Technologies) was used as the transfection reagent, according to the manufacturer's instructions. Cells were harvested after 48 h post transfection. Informed consent was obtained for all tissue donors, and all clinical investigation have been conducted according to the principles expressed in the Declaration of Helsinki.

ATP depletion and recovery assay

The ATP depletion and recovery assay was performed as described previously (Svitkina et al., 1986). Cells were incubated in phosphate-buffered saline (PBS) supplemented with 1 mM $CaCl_2$, 1 mM $MgCl_2$ and 20 mM NaN_3 for 1 h. This treatment causes a rapid depletion of the cellular ATP, inducing a reversible disassembly of actin filaments. NaN_3-containing buffer was then replaced with fresh medium supplemented with heat inactivated 10% FBS for 30 min to allow ATP recovery, leading to a rapid restoration of actin cytoskeleton, which occurs as a synchronous burst of membrane protrusions.

Immunofluorescence and confocal laser scanning microscopy

Cells were fixed with 4% formaldehyde in PBS, permeabilized in 0.2% Nonidet P40 (Boehringer Mannheim) for 10 min, and blocked with 1% BSA in PBS at room temperature. Samples were incubated sequentially with the appropriate primary and secondary antibodies. Slides were mounted with ProLong with Dapi (Life Technologies), and examined by conventional epifluorescence microscope (Olympus BX51; Milano, Italy). Images were captured by a SPOT RT3 camera and elaborated by IAS software. For colocalization analysis, slides were examined by acquiring a *z*-series of 25 optical sections at 0.8 µm intervals, with a ×63/1.2 NA water-corrected oil immersion CApochromat lens, and a digital zoom of 3, with the confocal system TCS-SP5 (Leica Microsystems GmbH, Wetzlar, Germany). Orthogonal projections (of an *x*- or *z*-plane corresponding to a point on the *y*-axis) were calculated from a 20 µm *z*-stack. The quantification of SMN and S6, and SMN and phospho-S6 colocalization over membrane protrusions and cytoplasm was performed as previously described (Tcherkezian et al., 2010).

Western blot analysis

Protein extracts were loaded on pre-cast NuPAGE 4–12% gels (Life Technologies) and transferred onto nitrocellulose membranes (GE Healthcare; Milano, Italy). Immunodetection of the reactive bands was revealed by chemiluminescence (ECL kit, GE Healthcare).

Preparation of plasma membrane-enriched fractions

The preparation of plasma-membrane-enriched fraction was performed as previously described (Vachon et al., 1987) with little modification. Cells were lysed in buffer A (5 mM Tris-HCl pH 7.4, 1 mM EGTA, 1 mM DTT and 320 mM sucrose). Extracts were passed five times through a 26G needle and centrifuged at 1000 ***g*** for 10 min at 4°C. The supernatant was kept and the pellet was quickly vortexed in the presence of the original volume of lysis buffer and centrifugated at 1000 ***g*** for 10 min at 4°C. The two supernatants were pooled and centrifuged at 24,000 ***g*** for 20 min at 4°C in a Beckman SW41 rotor. The supernatant was discarded and the pellet was resuspended in 12 ml of buffer B (5 mM Tris-HCl pH 7.4, 1 mM EGTA and 1 mM DTT), and centrifuged at 24,000 ***g*** for 30 min at 4°C at in a Beckman SW41 rotor. The supernatant was discarded and the pellet was processed in lysis buffer (100 mM Tris-HCl pH 8.0, 150 mM NaCl, 5 mM EDTA, 1% Triton X-100). The protein extract was processed for western blot analysis.

DRM preparation

The isolation of DRM fractions, containing lipid rafts, was performed as previously described (Clement et al., 2010).

Co-immunoprecipitation assay

For co-immunoprecipitation experiments, plasma-membrane-enriched fractions were resuspended in immunoprecipitation buffer [50 mM Tris-HCl pH 7.4, 250 mM NaCl, 5 mM EDTA, 0.1% Triton X-100, 5% glycerol and complete protease inhibitor cocktail (Roche)]. Extracts were passed five times through a 25G needle, incubated on ice for 15 min, and clarified at 9000 ***g*** for 15 min at 4°C. 250 µg of extract was immunoprecipitated in immunoprecipitation buffer with 1 µg of caveolin-1 polyclonal antibody or SMN monoclonal antibody, pre-adsorbed with anti-rabbit-IgG- or anti-mouse-IgG-conjugated magnetic beads (New England BioLabs) for 3 hours at 4°C. The same amount of non-specific IgG was used as control. After five washes with immunoprecipitation buffer, complexes were eluted by boiling in Laemmli's buffer and analysed by SDS-PAGE on 10% polyacrylamide gels followed by immunoblotting.

In situ proximity ligation assay

Cultures, treated as indicated were immediately fixed in 4% PFA for 15 min and thereafter subject to *in situ* PLA using Duolink In Situ Detection Reagents Red kit (DUO92008, Sigma-Aldrich), according to the manufacturer's instructions. Different combinations of primary antibodies to SMN and caveolin-1 were used. Then, PLA signals were detected by a TCS SP5 confocal laser scanning microscope (Leica Mycrosystems) using an 63×1.35 NA oil immersion objective. High-resolution images were acquired as a *z*-stack with a 0.5 µm z-interval. Two-dimensional projections at maximum intensity of each *z*-series were generated with the LAS AF software platform (Leica Microsystems). High-resolution (taken using a 63×, 1.35 NA objective) images from single scans were analysed by ImageJ (NIH) to calculate the density of PLA puncta.

Primary neuron cultures and treatments

Spinal cords were obtained from embryonic day 13 fetal rats. After removal of the dorsal root ganglia, spinal cords were dissected, washed with 5 ml of Earl's Balanced Salt Solution (Gibco), and centrifuged for 2 min at 150 ***g***. The tissue was resuspended and incubated for 15 min at 37°C with 0.02% trypsin followed by addition of DNase I (80 µg/ml) and trypsin inhibitor (0.52 mg/ml). Digested tissues were mechanically dissociated and centrifuged at 150 ***g*** for 10 min. The dissociated cells were plated at a density of 12×10^4 cells/cm^2 in neurobasal media supplemented with B27 (Gibco). For BDNF stimulation, neuron cultures at 3 days *in vitro* (DIV) were incubated for 30 min in neurobasal media, and then stimulated with 10 ng/ml BDNF (Prepotech) for 15 min. Fixed neurons were processed for the *in situ* PLA assay.

Preparation of nick-translated probe

One digoxigenin-labelled oligonucleotide probe was used to detect human β-actin mRNA. The probe was obtained by PCR amplification of human

Journal of Cell Science

cDNA using the following oligonucleotides: forward, 5′-ACACCCGCC-GCCAGCTCACCATGGA-3′; reverse, 5′-CCAGGTCCAGACGCAGGA-TGGCATG-3′. Digoxigenin (DIG)-labelled DNA probe was generated using a DIG-Nick Translation Mix Kit (Roche) according to the manufacturer's instruction.

Fluorescent *in situ* hybridization

Fibroblasts, subjected to ATP depletion and recovery assay, were processed for immunofluorescence, as above reported. FISH was performed as previously described, with little modification (Welshhans and Bassell, 2011). Briefly, cells were fixed in 4% formaldehyde, rinsed three times in PBS containing $MgCl_2$, permeabilized in 0.2% Nonidet P40 for 5 min and equilibrated in 1× SSC and pre-hybridized with hybridization buffer (40% formamide, 10% dextran sulfate, 4 mg/ml bovine serum albumin, 2× SSC, 1× PBS) for 1 h at 37°C. Then, cells were incubated overnight with DIG-labelled oligonucleotide probe in hybridization buffer at 37°C, rinsed with 40% formamide and 1×SSC (two times, 20 min each) at 37°C, five times with 1× SSC (two rinses for 15 min each and three rinses for 5 min each) at room temperature. Cells were washed three times with PBS containing $MgCl_2$ and incubated with anti-digoxigenin antibody for 2 h at room temperature, followed by Alexa-Fluor-594-conjugated secondary antibody incubation, for 45 min at room temperature, and mounted with ProLong with Dapi (Life Technologies). Stacks of images of membrane protrusions were acquired, and images were analysed using ImageJ.

SUnSET assay

The SUnSET assay was performed as previously described (Schmidt et al., 2009). Briefly, cells were subjected to the ATP depletion and recovery assay, in the presence or absence of 10 nM rapamycin. 10 µM of puromycin was added for an additional 10 min following the ATP recovery. Cells were harvested and processed for western blot analysis by using anti-puromycin antibody. Immunoblotting images were quantified by ImageJ. For experiments in which an immunofluorescence step was combined to the SUnSET assay, after ATP depletion and recovery assay, cells were incubated with 10 µM puromycin for 5 min. Samples were washed twice in ice-cold PBS supplemented with 355 µM cycloheximide, and then incubated on ice in PBS containing 0.002% Nonidet P-40 (Boehringer Mannheim), for 30 s, followed by rapid washing in ice-cold PBS. Cells were then fixed and processed for immunofluorescence as described above.

Statistical analysis

Data are presented as mean±s.d. or s.e.m. Statistical significance between groups was determined using the GraphPad Prism software. The unpaired *t*-test was performed to assess the significance; $P<0.05$ was considered statistically significant.

Acknowledgements

We thank Dr T. Costa and Dr M. Caruso for helpful discussion and critical reading of the manuscript. We thank Dr I. Pagano for technical assistance. We are also grateful to Dr R. Butler for the careful editing of the manuscript.

Competing interests

The authors declare no competing or financial interests.

Author contributions

M.G.D.C. designed experiments and wrote the manuscript. F.G. performed ATP depletion and recovery assays, plasma membrane preparations, transfection, western blotting, and co-immunoprecipitation and immunofluorescence experiments. C. Pisani performed FISH analysis, western blotting. M.T.C. performed primary neuron cultures and treatments. A.B., A.O. and T.I. performed data collections. S.F.-V. performed confocal microscopy. N. Canu performed the PLA analysis. L.M., N. Corbi and M.A.-T. provided reagents, materials and tools. C. Passananti supervised and provided guidance and crucial input into the study. All authors read and approved the final version of the manuscript.

Funding

This research was supported by FARMM onlus; Filas-Regione Lazio funding 'Sviluppo della Ricerca sul Cervello'; and Association Française contre les Myopathies [grant number 15586 to L.M.].

Supplementary information

Supplementary information available online at
http://jcs.biologists.org/lookup/suppl/doi:10.1242/jcs.176750/-/DC1

References

Bassell, G. J. and Warren, S. T. (2008). Fragile X syndrome: loss of local mRNA regulation alters synaptic development and function. *Neuron* **60**, 201-214.

Bear, J. E., Svitkina, T. M., Krause, M., Schafer, D. A., Loureiro, J. J., Strasser, G. A., Maly, I. V., Chaga, O. Y., Cooper, J. A., Borisy, G. G. et al. (2002). Antagonism between Ena/VASP proteins and actin filament capping regulates fibroblast motility. *Cell* **109**, 509-521.

Béchade, C., Rostaing, P., Cisterni, C., Kalisch, R., La Bella, V., Pettmann, B. and Triller, A. (1999). Subcellular distribution of survival motor neuron (SMN) protein: possible involvement in nucleocytoplasmic and dendritic transport. *Eur. J. Neurosci.* **11**, 293-304.

Berven, L. A., Willard, F. S. and Crouch, M. F. (2004). Role of the p70(S6K) pathway in regulating the actin cytoskeleton and cell migration. *Exp. Cell Res.* **296**, 183-195.

Besse, F. and Ephrussi, A. (2008). Translational control of localized mRNAs: restricting protein synthesis in space and time. *Nat. Rev. Mol. Cell Biol.* **9**, 971-980.

Bryant, D. M. and Mostov, K. E. (2008). From cells to organs: building polarized tissue. *Nat. Rev. Mol. Cell Biol.* **9**, 887-901.

Clement, A. B., Gimpl, G. and Behl, C. (2010). Oxidative stress resistance in hippocampal cells is associated with altered membrane fluidity and enhanced nonamyloidogenic cleavage of endogenous amyloid precursor protein. *Free Radic. Biol. Med.* **48**, 1236-1241.

Darnell, J. C., Van Driesche, S. J., Zhang, C., Hung, K. Y. S., Mele, A., Fraser, C. E., Stone, E. F., Chen, C., Fak, J. J., Chi, S. W. et al. (2011). FMRP stalls ribosomal translocation on mRNAs linked to synaptic function and autism. *Cell* **146**, 247-261.

De Rubeis, S., Pasciuto, E., Li, K. W., Fernández, E., Di Marino, D., Buzzi, A., Ostroff, L. E., Klann, E., Zwartkruis, F. J. T., Komiyama, N. H. et al. (2013). CYFIP1 coordinates mRNA translation and cytoskeleton remodeling to ensure proper dendritic spine formation. *Neuron* **79**, 1169-1182.

Delanote, V., Vandekerckhove, J. and Gettemans, J. (2005). Plastins: versatile modulators of actin organization in (patho)physiological cellular processes. *Acta Pharmacol. Sin.* **26**, 769-779.

Dimitriadi, M., Sleigh, J. N., Walker, A., Chang, H. C., Sen, A., Kalloo, G., Harris, J., Barsby, T., Walsh, M. B., Satterlee, J. S. et al. (2010). Conserved genes act as modifiers of invertebrate SMN loss of function defects. *PLoS Genet.* **6**, e1001172.

Dombert, B., Sivadasan, R., Simon, C. M., Jablonka, S. and Sendtner, M. (2014). Presynaptic localization of Smn and hnRNP R in Axon terminals of embryonic and postnatal mouse motoneurons. *PLoS ONE* **9**, e110846.

Dubroca, C., Loyer, X., Retailleau, K., Loirand, G., Pacaud, P., Feron, O., Balligand, J. L., Lévy, B. I., Heymes, C. and Henrion, D. (2007). RhoA activation and interaction with Caveolin-1 are critical for pressure-induced myogenic tone in rat mesenteric resistance arteries. *Cardiovasc. Res.* **73**, 190-197.

Fallini, C., Zhang, H., Su, Y., Silani, V., Singer, R. H., Rossoll, W. and Bassell, G. J. (2011). The survival of motor neuron (SMN) protein interacts with the mRNA-binding protein HuD and regulates localization of poly(A) mRNA in primary motor neuron axons. *J. Neurosci.* **31**, 3914-3925.

Fallini, C., Bassell, G. J. and Rossoll, W. (2012). Spinal muscular atrophy: the role of SMN in axonal mRNA regulation. *Brain Res.* **1462**, 81-92.

Fallini, C., Rouanet, J. P., Donlin-Asp, P. G., Guo, P., Zhang, H., Singer, R. H., Rossoll, W. and Bassell, G. J. (2014). Dynamics of survival of motor neuron (SMN) protein interaction with the mRNA-binding protein IMP1 facilitates its trafficking into motor neuron axons. *Dev. Neurobiol.* **74**, 319-332.

Fan, L. and Simard, L. R. (2002). Survival motor neuron (SMN) protein: role in neurite outgrowth and neuromuscular maturation during neuronal differentiation and development. *Hum. Mol. Genet.* **11**, 1605-1614.

Gibbings, D. J., Ciaudo, C., Erhardt, M. and Voinnet, O. (2009). Multivesicular bodies associate with components of miRNA effector complexes and modulate miRNA activity. *Nat. Cell Biol.* **11**, 1143-1149.

Glinka, M., Herrmann, T., Funk, N., Havlicek, S., Rossoll, W., Winkler, C. and Sendtner, M. (2010). The heterogeneous nuclear ribonucleoprotein-R is necessary for axonal beta-actin mRNA translocation in spinal motor neurons. *Hum. Mol. Genet.* **19**, 1951-1966.

Gracias, N. G., Shirkey-Son, N. J. and Hengst, U. (2014). Local translation of TC10 is required for membrane expansion during axon outgrowth. *Nat. Commun.* **5**, 3506.

Grande-García, A., Echarri, A., de Rooij, J., Alderson, N. B., Waterman-Storer, C. M., Valdivielso, J. M. and del Pozo, M. A. (2007). Caveolin-1 regulates cell polarization and directional migration through Src kinase and Rho GTPases. *J. Cell Biol.* **177**, 683-694.

Hamilton, G. and Gillingwater, T. H. (2013). Spinal muscular atrophy: going beyond the motor neuron. *Trends Mol. Med.* **19**, 40-50.

Hao, L. T., Wolman, M., Granato, M. and Beattie, C. E. (2012). Survival motor neuron affects plastin 3 protein levels leading to motor defects. *J. Neurosci.* **32**, 5074-5084.
Hérincs, Z., Corset, V., Cahuzac, N., Furne, C., Castellani, V., Hueber, A.-O. and Mehlen, P. (2005). DCC association with lipid rafts is required for netrin-1-mediated axon guidance. *J. Cell Sci.* **118**, 1687-1692.
Hoeffer, C. A. and Klann, E. (2010). mTOR signaling: at the crossroads of plasticity, memory and disease. *Trends Neurosci.* **33**, 67-75.
Holt, C. E. and Bullock, S. L. (2009). Subcellular mRNA localization in animal cells and why it matters. *Science* **326**, 1212-1216.
Hubers, L., Valderrama-Carvajal, H., Laframboise, J., Timbers, J., Sanchez, G. and Côté, J. (2011). HuD interacts with survival motor neuron protein and can rescue spinal muscular atrophy-like neuronal defects. *Hum. Mol. Genet.* **20**, 553-579.
Jung, H., Gkogkas, C. G., Sonenberg, N. and Holt, C. E. (2014). Remote control of gene function by local translation. *Cell* **157**, 26-40.
Kalinowska, M., Castillo, C. and Francesconi, A. (2015). Quantitative profiling of brain lipid raft proteome in a mouse model of fragile X syndrome. *PLoS ONE* **10**, e0121464.
Kong, L., Wang, X., Choe, D. W., Polley, M., Burnett, B. G., Bosch-Marcé, M., Griffin, J. W., Rich, M. M. and Sumner, C. J. (2009). Impaired synaptic vesicle release and immaturity of neuromuscular junctions in spinal muscular atrophy mice. *J. Neurosci.* **29**, 842-851.
Kwiatkowski, T. J., Jr., Bosco, D. A., Leclerc, A. L., Tamrazian, E., Vanderburg, C. R., Russ, C., Davis, A., Gilchrist, J., Kasarskis, E. J., Munsat, T. et al. (2009). Mutations in the FUS/TLS gene on chromosome 16 cause familial amyotrophic lateral sclerosis. *Science* **323**, 1205-1208.
Kye, M. J., Niederst, E. D., Wertz, M. H., Gonçalves, I. d. C. G., Akten, B., Dover, K. Z., Peters, M., Riessland, M., Neveu, P., Wirth, B. et al. (2014). SMN regulates axonal local translation via miR-183/mTOR pathway. *Hum. Mol. Genet.* **23**, 6318-6331.
Latham, V. M., Jr., Kislauskis, E. H., Singer, R. H. and Ross, A. F. (1994). Beta-actin mRNA localization is regulated by signal transduction mechanisms. *J. Cell Biol.* **126**, 1211-1219.
Lee, Y. S., Pressman, S., Andress, A. P., Kim, K., White, J. L., Cassidy, J. J., Li, X., Lubell, K., Lim, D. H., Cho, I. S. et al. (2009). Silencing by small RNAs is linked to endosomal trafficking. *Nat. Cell Biol.* **11**, 1150-1156.
Li, D. K., Tisdale, S., Lotti, F. and Pellizzoni, L. (2014). SMN control of RNP assembly: from post-transcriptional gene regulation to motor neuron disease. *Semin. Cell Dev. Biol.* **32**, 22-29.
Medioni, C., Mowry, K. and Besse, F. (2012). Principles and roles of mRNA localization in animal development. *Development* **139**, 3263-3276.
Napoli, I., Mercaldo, V., Boyl, P. P., Eleuteri, B., Zalfa, F., De Rubeis, S., Di Marino, D., Mohr, E., Massimi, M., Falconi, M. et al. (2008). The fragile X syndrome protein represses activity-dependent translation through CYFIP1, a new 4E-BP. *Cell* **134**, 1042-1054.
Oprea, G. E., Kröber, S., McWhorter, M. L., Rossoll, W., Müller, S., Krawczak, M., Bassell, G. J., Beattie, C. E. and Wirth, B. (2008). Plastin 3 is a protective modifier of autosomal recessive spinal muscular atrophy. *Science* **320**, 524-527.
Pan, F., Hüttelmaier, S., Singer, R. H. and Gu, W. (2007). ZBP2 facilitates binding of ZBP1 to beta-actin mRNA during transcription. *Mol. Cell. Biol.* **27**, 8340-8351.
Pellizzoni, L., Yong, J. and Dreyfuss, G. (2002). Essential role for the SMN complex in the specificity of snRNP assembly. *Science* **298**, 1775-1779.
Peter, C. J., Evans, M., Thayanithy, V., Taniguchi-Ishigaki, N., Bach, I., Kolpak, A., Bassell, G. J., Rossoll, W., Lorson, C. L., Bao, Z.-Z. et al. (2011). The COPI vesicle complex binds and moves with survival motor neuron within axons. *Hum. Mol. Genet.* **20**, 1701-1711.
Rathod, R., Havlicek, S., Frank, N., Blum, R. and Sendtner, M. (2012). Laminin induced local axonal translation of β-actin mRNA is impaired in SMN-deficient motoneurons. *Histochem. Cell Biol.* **138**, 737-748.
Ridley, A. J. (2011). Life at the leading edge. *Cell* **145**, 1012-1022.
Rinaldo, C., Moncada, A., Gradi, A., Ciuffini, L., D'Eliseo, D., Siepi, F., Prodosmo, A., Giorgi, A., Pierantoni, G. M., Trapasso, F. et al. (2012). HIPK2 controls cytokinesis and prevents tetraploidization by phosphorylating histone H2B at the midbody. *Mol. Cell* **47**, 87-98.
Rossoll, W., Jablonka, S., Andreassi, C., Kröning, A. K., Karle, K., Monani, U. R. and Sendtner, M. (2003). Smn, the spinal muscular atrophy-determining gene product, modulates axon growth and localization of beta-actin mRNA in growth cones of motoneurons. *J. Cell Biol.* **163**, 801-812.
Sanchez, G., Dury, A. Y., Murray, L. M., Biondi, O., Tadesse, H., El Fatimy, R., Kothary, R., Charbonnier, F., Khandjian, E. W. and Côté, J. (2013). A novel function for the survival motoneuron protein as a translational regulator. *Hum. Mol. Genet.* **22**, 668-684.
Schmidt, E. K., Clavarino, G., Ceppi, M. and Pierre, P. (2009). SUnSET, a nonradioactive method to monitor protein synthesis. *Nat. Methods* **6**, 275-277.
Schuck, S., Honsho, M., Ekroos, K., Shevchenko, A. and Simons, K. (2003). Resistance of cell membranes to different detergents. *Proc. Natl. Acad. Sci. USA* **100**, 5795-5800.
Svitkina, T. M., Neyfakh, A. A., Jr. and Bershadsky, A. D. (1986). Actin cytoskeleton of spread fibroblasts appears to assemble at the cell edges. *J. Cell Sci.* **82**, 235-248.
Tadesse, H., Deschênes-Furry, J., Boisvenue, S. and Côté, J. (2008). KH-type splicing regulatory protein interacts with survival motor neuron protein and is misregulated in spinal muscular atrophy. *Hum. Mol. Genet.* **17**, 506-524.
Tcherkezian, J., Brittis, P. A., Thomas, F., Roux, P. P. and Flanagan, J. G. (2010). Transmembrane receptor DCC associates with protein synthesis machinery and regulates translation. *Cell* **141**, 632-644.
Vachon, L., Costa, T. and Herz, A. (1987). GTPase and adenylate cyclase desensitize at different rates in NG108-15 cells. *Mol. Pharmacol.* **31**, 159-168.
Welshhans, K. and Bassell, G. J. (2011). Netrin-1-induced local β-actin synthesis and growth cone guidance requires zipcode binding protein 1. *J. Neurosci.* **31**, 9800-9813.
Willett, M., Brocard, M., Pollard, H. J. and Morley, S. J. (2013). mRNA encoding WAVE–Arp2/3-associated proteins is co-localized with foci of active protein synthesis at the leading edge of MRC5 fibroblasts during cell migration. *Biochem. J.* **452**, 45-55.
Willis, D. E., van Niekerk, E. A., Sasaki, Y., Mesngon, M., Merianda, T. T., Williams, G. G., Kendall, M., Smith, D. S., Bassell, G. J. and Twiss, J. L. (2007). Extracellular stimuli specifically regulate localized levels of individual neuronal mRNAs. *J. Cell Biol.* **178**, 965-980.
Wodarz, A. (2002). Establishing cell polarity in development. *Nat. Cell Biol.* **4**, E39-E44.
Xing, L. and Bassell, G. J. (2013). mRNA localization: an orchestration of assembly, traffic and synthesis. *Traffic* **14**, 2-14.
Yamazaki, T., Chen, S., Yu, Y., Yan, B., Haertlein, T. C., Carrasco, M. A., Tapia, J. C., Zhai, B., Das, R., Lalancette-Hebert, M. et al. (2012). FUS-SMN protein interactions link the motor neuron diseases ALS and SMA. *Cell Rep.* **2**, 799-806.
Yasuda, K., Zhang, H., Loiselle, D., Haystead, T., Macara, I. G. and Mili, S. (2013). The RNA-binding protein Fus directs translation of localized mRNAs in APC-RNP granules. *J. Cell Biol.* **203**, 737-746.
Zhang, H. L., Pan, F., Hong, D., Shenoy, S. M., Singer, R. H. and Bassell, G. J. (2003). Active transport of the survival motor neuron protein and the role of exon-7 in cytoplasmic localization. *J. Neurosci.* **23**, 6627-6637.